JOURNAL OF COMPUTATIONAL PHYSICS 105, 187–198 (1993)

A Conservative Stable Smoothness-Enhancing Free-Lagrangian Method

V. M. HAZINS AND V. V. SVETSOV

Institute for Dynamics of Geospheres, Russian Academy of Sciences, Moscow 117 979, Russia

Received January 27, 1991; revised July 13, 1992

In this paper a two-dimensional free-Lagrangian method for modeling compressible fluid flows is presented. Within the traditional general approach, combining a flexible reconnected triangular mesh with a finite difference algorithm, several new important numerical techniques are developed to enhance stability and smoothness of the method. Characteristic features of the method are a new technique of additional mesh connections and a way of mapping variables from nodes to zones and back. A finite difference scheme is chosen to conserve different forms of energy. The implicit discrete equations are solved by a special iterative procedure. Four numerical examples, including flows with relatively complex internal structure, are considered. © 1993 Academic Press, Inc.

1. INTRODUCTION

The Lagrangian formulation has obvious advantages for a large variety of physical problems including interfaces, free surfaces, confined masses of moving fluids, as well as changes of a material state—chemical or kinetic reactions. This stimulates a continual development of free-Lagrangian methods. Experience accumulated in two and three dimensions and the codes developed recently enable one to obtain numerical solutions of sufficiently difficult fluid flow problems (see [1–4]). The current extensions of the method are based on different forms of the mesh, different discretizations of governing equations, and different techniques of mesh reconnection caused by the relative displacement of fluid elements. Sometimes a mesh refinement is used to adapt the mesh to the gradients of the variables. That is, an extensive technology is available for calculations.

But, as a matter of fact, free-Lagrangian methods are less advanced and investigated than Eulerian, Lagrangian–Eulerian, or particle-in-cell methods. The problems solved numerically usually have, if interfaces are not to be taken into account, a simpler internal structure of the flow than in a great number of problems solved by other methods. The accuracy and convergence of numerical solutions have been studied in detail, mainly for one-dimensional geometry; see, e.g., [5]. We believe this situation is caused not only by the more expensive calculations but mainly by the intrinsic difficulties of the free-Lagrangian methods. This particularly concerns the process of mesh reconnection accompanied by changes of the point neighborhood. Such a process seems to insert an additional unknown mechanism which is not described by the fluid dynamics equations and stimulates perturbations. Since the natural numerical viscosity of the free-Lagrangian methods is not usually large, points can acquire additional chaotic small-scale motions and undesirable penetrative properties. These perturbations distort the solution and can lead to an inadequate description of the physical process.

For this reason not only various types of artificial viscosity are widely used in free-Lagrangian methods [6], but, in addition, artificial velocities [3], an artificial improvement of nodal locations [7], restrictions of particle penetrations [8], and some other artificial dissipators. The Lagrangian–Eulerian methods mitigate the difficulties by the rezoning phase, that is, a periodical transference of the variables into a new mesh. Evidently, this approach gives a smoothing effect, introducing, similar to the Eulerian methods, a numerical diffusion. A finite difference scheme is very important from this point of view. That is why the schemes having an enlarged numerical viscosity, e.g., the Godunov method, lead to robust codes [9]. We believe that to obtain a robust code without any auxiliary artificial remedies that smooth and stable difference schemes should be used. The perturbations caused by the mesh reconnections should also be reduced to a minimum.

We made an attempt to overcome the difficulties of the free-Lagrangian method. The proposed two-dimensional conservative stable smoothness-enhancing free-Lagrangian method (CSSEL) is constructed in such a way as to enhance smoothness and stability of the numerical solution in different aspects.

First, the triangular mesh is used with all the variables node-centered. Following the idea [6] with certain modifications, temporary zone-centered energies and masses are introduced by a mapping process. The pressure becomes also zone-centered, so that the triangles make the

0021-9991/93 $5.00

mesh stiffer and more stable to perturbations. In contrast to [1] we consider the mesh stiffness, as a technique for the suppression of perturbations, to have a great advantage, especially for flows with a complex structure. In addition, the schemes with node-centered velocities and zone-centered pressures favor a smoothness of calculations. (We tried and abandoned Voronoi cells because our numerical tests of such an approach with all variables zone-centered have revealed some disadvantages. The major one is that points under compression can come too close together.)

Second, the templates for the discrete equations include both the nearest neighbors of the node defined by the Voronoi algorithm and the neighbors of the nearest neighbors if they are sufficiently close. This permits the points to interact before they become the nearest neighbors and improves the method itself.

Third, great attention is paid to the conservative properties of the scheme. The finite difference scheme we have chosen has been proposed in [10] for node-centered velocities and zone-centered pressures. The discrete equations conserve total energy and momentum, as well as include the exact local relationships between internal, kinetic, and total energies. This is especially important for problems with kinetic-into-internal energy transformations, as well for a coarse mesh. We have combined the scheme [10] with the process of mapping the mass and energy from nodes to zones.

And finally, we enhance the stability of the finite difference scheme itself by introducing implicit terms into the motion equation. To solve the discrete equations an iterative process is designed.

The strength and possibilities of CSSEL are demonstrated by several computational examples, including an interaction of a shock wave, caused by an impulsive load, with a thin gas layer of low density, a Meshkov–Richtmyer instability, a high speed projectile impact on a material surface, and jet formation resulting from the expansion of a vaporized foil.

The algorithm can be divided into sequantial steps: reconnection (triangulation and additional connections), mapping, hydrodynamics, and remapping.

2. MESH ORGANIZATION

2.1. *Triangulation*

In our method the Delaunay triangular mesh [11], dual to the Voronoi mesh [12], is employed. This technique of triangulation is widely known and needs no special description.

We did not use any of the algorithms for initial mesh generation because at the beginning the points were regularly distributed and could be easily connected in a proper way. As the problem runs, the simple frequently used technique of maintaining the Delaunay mesh is employed (see [1, 13]). It works in the following way. The triangles which have a common side are examined at every cycle. If the sum of the angles opposite to the common side exceeds 180° the existent common side (a diagonal of the quadrilateral) is removed and the other diagonal is used as a connector.

It should be pointed out that triangular cells can become largely stretched along some directions during calculation. Or it can prove convenient to specially construct a stretched or compressed grid. As a result of small point displacements and the following restructuring of such a mesh in accordance with the Delaunay triangulation, small triangle areas can arise. In this case it is often reasonable to keep the stretched cells for an approximation improvement. For this purpose the Delaunay triangulation is applied to the compressed cells. A center of the quadrilateral formed by the triangles and a strething direction are defined for every pair of neighboring triangles. (The center of the quad is defined as a mass center and the stretching direction is defined by the extreme value of the quad moment of inertia along this direction). Then the neighbor change criterion described above is applied in the coordinate system which is located in the quad center, has an axis along the stretching direction, and is compressed along the appropriate direction so that the quad has an approximately equal size along both axes.

If a problem includes rigid walls, a moving piston, or symmetry axes, no nodes are located on the boundaries. Auxiliary fictitious nodes that are symmetrical to the wall or the axis are introduced into the Delaunay mesh. This provides an appropriate approximation of the boundary conditions and a uniform calculation process for all triangles and interior nodes. The mass, energy, and density at the fictitious points are set equal to the values at the corresponding symmetrical interior nodes. Interfaces and free surfaces are not specified. The motion of the free surface points occurs due to the absence of neighbors on the vacuum side.

It should be specially noted that points in the real fluid flow can escape either to the free boundary or migrate out of it to the interior region. To take this process into account the free surface is examined during a calculation. If three neighboring points belonging to the free surface can form an acute triangle this triangle is created with the middle point becoming interior. The reverse process goes as follows: If two boundary points and an interior point form a triangle with an angle larger than 120° this triangle is broken so that each of the three points now belongs to the free boundary.

2.2. *Additional Connections*

Switches of diagonals in the quadrilaterals during reconnections result in discontinuous acceleration. In fact, a

formation of new triangles with their new zone-centered parameters is discontinuous. The points start to interact only at a fairly close distance after they become the nearest neighbors. The effective nodal surface is changed discontinuously and this also may cause undesirable perturbations.

Note that the point acceleration is continuous if the Voronoi polygonal cells are used as the integration control volumes because the length of the polygon side between two points which have just become nearest neighbors (and hence the contribution of this side to the integral) proves to be zero. For this reason the action of the new nearest neighbor on the point just after reconnection is small. Nevertheless, such a mechanism of the interaction of points seems to start too late and does not cause an appropriate pressure rise in the cell to provide a reflection in all the cases when the particles collide.

We have designed a technique reducing the discontinuities during reconnections in our approach and enhancing the smoothing and monotonic properties of the method. We let the points interact before they become the nearest neighbors. In this way certain joint triangles, called couples, are chosen from all the variety of triangles. Two triangles forming a couple have to satisfy the following three conditions. First, these triangles are required to form a convex quadrilateral (none of its four angles exceeds 180°). Second, a sum of two angles opposite to the common side (denote this sum by φ) must be greater than the similar sums for the other quadrilaterals formed by each of the two triangles. And third, φ must be greater than the quantity φ_0 (which is taken to be 90°). Thus, the couples consist of the traingles which are to be reconstructed in the following cycles. Some triangles may not be included in the couples. In the quadrilateral formed by the couple an additional diagonal is created.

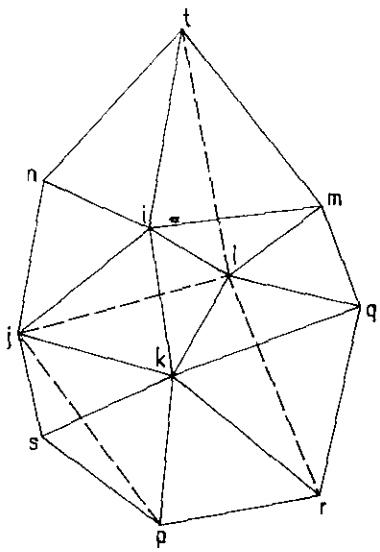

FIG. 1. An example of the triangular mesh. The Delanay triangulation is shown by solid lines. The additional connections are shown by dashed lines.

Connections of triangles in the couples are illustrated in Fig. 1. The normal triangular grid is shown by solid lines. We will try to make some explanations based on this figure. Triangle Δijk is the only one for triangle Δikl to form a couple. Triangle Δmil does not match Δikl because quad $mikl$ is concave; neither does triangle Δqlk. For triangle Δijk there are three possibilities to form a couple. But triangle Δijk forms it with Δikl since the sum φ of angles j and l is greater than the sum of angles n and k and the sum of angles i and s. Triangles Δnji and Δnit do not form a couple because the sum φ is smaller than 90°. Triangles Δprk and Δlqm do not have any free adjoining triangle, so they can not form a couple.

The idea is that not only the triangles of the main grid but also the triangles formed by additional connections are simultaneously involved in the calculation. The mapping procedure is applied for each triangle independently, but the contributions to the node-centered velocity increments after the momentum equation is solved and to the node energy at the remapping stage are multiplied by the coupling coefficients which are introduced in the following way. For example, for triangles Δijk and Δikl the coefficient is taken to be

$$c_1 = 1 + 0.5 \cos \varphi, \tag{1}$$

where φ is the sum of angles j and l. For triangles Δijl and Δjkl the coefficient is introduced as

$$c_2 = -0.5 \cos \varphi. \tag{2}$$

Other forms of c_1 and c_2 are possible, but it is important to satisfy the following conditions:

$$\begin{aligned} &c_1 + c_2 = 1, \\ &c_1 = c_2 = 0.5, \qquad \text{if} \quad \varphi = 180°, \\ &c_1 = 1,\ c_2 = 0, \qquad \text{if} \quad \varphi > \varphi_0. \end{aligned}$$

The value φ_0 defines the neighbors which the node can "feel." In this way, for example, the force on node 1 is determined not only by surrounding nodes i, k, q, m but, in addition, by nodes j, r, and t.

The technique described here works as if the calculations were made twice for two different meshes (consisting of solid lines and of solid and dashed lines), and the resulting variables values were obtained by summation with the weighting coefficients. The result is that the reconnections (in accordance with the Delaunay triangulation) do not have an appreciable effect on the calculated variables. For the couple of right triangles it does not matter which of the

two possible diagonals is used. Therefore, the triangulated orthogonal grid with eight neighbors to every point (including additional connections) becomes the most suitable for calculations. (In the absence of additional connections the orthogonal triangulated grid with six neighbors to every point is not convenient because a reconstruction takes place at small node displacements that can lead to oscillations.)

2.3. *Mapping Procedure*

In our method all prognostic variables (specific energies e_i, particle coordinates $\mathbf{r}_i$, and velocities $\mathbf{u}_i$) are point-centered. Masses m_i associated with nodes are constant for all time. Following [6], the mapping procedure is performed at the beginning of each cycle; that is, temporary zone-centered energies and masses are computed. The zone-centered information is forgotten at the end of each cycle. The calculated zone-centered energy increments are contributed back to the nodes at the remapping stage with a conservation of the internal energy.

We have modified the mapping procedure to enhance the smoothness of the method. In [6] the mass and energy contributions from a point to zones have been taken proportional to the angles between the triangles sides coming from the node. We put the mass and energy contributions from the node to every zone to be equal; that is, the mass of the node is divided equally among the triangles surrounding the node. This makes the mesh stiffer and more sensitive to the changes of variables and prevents a chaotic motion. The density and specific energy grow sharply if the triangle compresses and its area reduces. Another advantage of this mapping technique is that the triangular zones have fixed masses in the absence of reconnections.

The mapping phase can be specified by

$$\begin{aligned} m_k &= \sum_{j(k)} \frac{m_j}{N_j} \\ m_k e_k &= \sum_{j(k)} \frac{m_j e_j}{N_j}, \end{aligned} \tag{3}$$

where k represents the triangular zone, j represents the node, N_j is the number of triangles surrounding node j, and $j(k)$ are the nodes associated with triangle k. Note that here and below subscript k refers to zones, and subscripts i and j refer to nodes.

The pressure at nodes and zones is calculated through the equation of state. However, to prevent the extreme growth of the zone-centered pressure its value in each zone is restricted by the maximum pressure at the vertices. The major difficulty of this approach appears for problems with several materials. It is not quite clear how to calculate the pressure in a zone if the triangle is comprised of mass elements which belong to different materials.

In the example calculations demonstrated below we took the same equation of state for different gases. But recently we computed the penetration of a massive body into a light gas, assuming different equations of state. In this case we calculated the pressure in the triangles at the interface through the equation of state of the light gas even if an only node belonged to the gas. This produced good results, but the problem of equation of state stands and should be investigated more carefully.

3. THE FINITE DIFFERENCE APPROACH

3.1. *Discrete Equations*

Finite difference equations obtained in [10] from the variational principle can be written either for Cartesian or cylindrical geometries. The density ρ_k and volume V_k of the triangular zone k are defined as

$$m_k = V_k \rho_k, \tag{4}$$

$$V_k = \frac{1}{2\alpha}\left((x_{i_2}^{\alpha} - x_{i_1}^{\alpha})(y_{i_3} - y_{i_1}) - (x_{i_3}^{\alpha} - x_{i_1}^{\alpha})(y_{i_2} - y_{i_1})\right), \tag{5}$$

where m_k is the zone-centered mass, x_i, y_i are the node coordinates, and $\alpha = 1$ or 2 for plane and cylindrical geometry, respectively. For cylindrical geometry x_i is the radius and y_i is the length along the symmetry axis. The vertices of the triangular zone k are denoted as i_1, i_2, i_3 in a counterclockwise order.

The momentum equation is written for node i as

$$m_i \frac{\mathbf{u}_i^{n+1} - \mathbf{u}_i^n}{\Delta t} = \sum_{k(i)} \tilde{P}_k \nabla_i V_k^{n+0.5}, \tag{6}$$

where m_i is the node mass, $\mathbf{u}_i$ is the velocity vector, Δt is the time-step, $\tilde{P}_k$ is the zone pressure, and ∇_i means gradient with respect to the coordinates of the particle i. Summation is done over all triangles surrounding the node i. The superscripts n and $n+1$ designate subsequent time levels. The superscript $n+0.5$ denotes time centering which has a special form for the volume derivatives

$$\begin{aligned} \frac{\partial V_k^{n+0.5}}{\partial x_i} &= \frac{1}{2}(x_i^{\alpha-1})^{n+0.5}(y_{i_1} - y_{i_2})^{n+0.5}, \\ \frac{\partial V_k^{n+0.5}}{\partial y_i} &= \frac{1}{2\alpha}(x_{i_2}^{\alpha} - x_{i_1}^{\alpha})^{n+0.5}, \end{aligned} \tag{7}$$

where i_1 and i_2 are the vertices of the triangle k sequentially numbered from the vertex i in a counterclockwise order.

Particle trajectories $\mathbf{r}(x, y)$ are calculated on the basis of the kinematic equation

$$\frac{\mathbf{r}_i^{n+1} - \mathbf{r}_i^n}{\Delta t} = \mathbf{u}_i^{n+0.5}. \tag{8}$$

The equation of the energy conservation can be written as

$$m_k \frac{e_k^{n+1} - e_k^n}{\Delta t} = -\tilde{P}_k \sum_{j(k)} \mathbf{u}_j^{n+0.5} \nabla_j V_k^{n+0.5}, \tag{9}$$

where e_k is the specific internal energy and the sum is over three vertices of the triangle k.

Time centering in Eqs. (6) to (9) is introduced in accordance with the ideas [14]. That is, Eq. (9) can be exactly transformed both into the thermodynamic equation for the specific internal energy

$$m_k \frac{e_k^{n+1} - e_k^n}{\Delta t} = -\tilde{P}_k \frac{V_k^{n+1} - V_k^n}{\Delta t}$$

and into same local relationship for a specific total energy. The summation of Eq. (6) multiplied by $\mathbf{u}_i^{n+0.5}$ over all nodes plus the summation of Eq. (9) over all zones gives an accurate conservation of the total energy.

Thus, the impulse and energy conservation is guaranteed in the finite difference equations. The correct approximation of the energy equation in various difference forms is very important. For the conservative schemes without these properties negative values of thermal energy may appear during the calculation.

Time centering of the zone pressure $\tilde{P}_k$, including the artificial viscosity, does not affect the energy conservation. But to obtain a greater stability an implicit scheme should be used. The pressure can be extrapolated from time level n to $n+1$ by assuming that the entropy of the particle is constant [15]. This leads to the expression

$$P_k^{n+1} = P_k^n + \left(\frac{\partial P}{\partial V}\bigg|_s\right)_k^n \frac{\partial V_k}{\partial t} \Delta t.$$

Then, the pressure in Eqs. (6) and (9) can be written as

$$\tilde{P}_k = P_k^n - \left(\frac{\rho_k c_k^2}{V_k}\right)^n \times \Delta t \sum_{j(k)} \mathbf{u}_j^{n+1} \nabla_j V_k^{n+0.5} + Q_k. \tag{10}$$

Here c_k is the sound speed, Q_k is the artificial viscosity, and P_k^n is the zone pressure which is determined from the equation of state

$$P_k^n = P_k^n(e_k^n, \rho_k^n). \tag{11}$$

As a result of such pressure extension to the next time level, Eq. (6) becomes implicit and the finite difference scheme becomes unconditionally stable. However, Eq. (6) must be solved by some iterative procedure which will be described in the following section.

Following [16], the artificial viscosity can be used in a form

$$Q_k = \varepsilon \rho_k^n \Delta u_k^2, \tag{12}$$

where ε is the numerical constant and Δu_k is the difference of velocity components at a distance of a cell size. If the cell volume grows, Q_k is set to be zero. However, for the two-dimensional geometry it is not quite clear in which way Δu_k should be determined. Requiring Q_k be invariant with respect to a grid compression or stretching, we calculate Δu_k in the following way: Every side of the triangle is considered. If the side is compressed the difference of velocities at every pair of vertices is taken and then Δu_k is defined as the maximum of three quantities:

$$\Delta u_k = \mathrm{Max}(|\mathbf{u}_{i_1}^n - \mathbf{u}_{i_2}^n|, |\mathbf{u}_{i_2}^n - \mathbf{u}_{i_3}^n|, |\mathbf{u}_{i_3}^n - \mathbf{u}_{i_1}^n|). \tag{13}$$

If the side of the triangle is stretched the corresponding difference in (13) is set to equal zero.

We tried other forms of artificial viscosity, for example, projecting of the velocity field onto the direction of velocity gradient. But this direction proved to be fairly close to the direction of the triangle side which is subjected to the maximum compression. The test calculation have shown that the simplified form of artificial viscosity (12), (13) does not make the results worse. But in some cases (12), (13) provides too much viscosity. To get the "best" form of viscosity more comprehensive investigations are necessary.

Assuming constant entropy as a model for pressure extrapolation in zones that are being shocked does not lead to any essential consequences because the pressure extrapolation is equivalent to some auxiliary artificial viscosity which is much smaller than the main artificial viscosity (12).

3.2. *Remapping*

After solving the system of Eqs. (4) to (13) at every time level, the remapping, that is, the contributions of the energy increments $\Delta e_k = e_k^{n+1} - e_k^n$ to the appropriate nodes, is applied. This procedure differs essentially from [6]. The value Δe_k is separated into two components Δe_k^1 and Δe_k^2. The first one Δe_k^1 is the energy increment caused by the artificial viscosity, and Δe_k^2 is cause by the work of the pressure itself. Contributions of the positive Δe_k^1 into the vertices are made proportionally to the densities at the vertices

$$\Delta e_i^1 = \frac{m_k \Delta e_k^1 \rho_i}{\sum_{j(k)} m_j \rho_j}. \tag{14}$$

This reduces the error in anomalous heating if shock formation takes place. (This defect is known to be inherent to Lagrangian schemes [5].)

Contributions of $m_k \Delta e_k^2$ into the nodes are made with some precautions to prevent an extreme heating or cooling. Namely, if Δe_k^2 is negative the contributions are made to the vertices with the maximum pressures at the previous time level. In the opposite case $m_k \Delta e_k^2$ is contributed to the vertices with the minimum node pressures. As the numerical tests have shown, this way of Δe_k contributions does not cause too strong smoothing, since the dependence of the variables for known simple problems was close to analytic solutions.

The remapping procedure is consistent with internal energy conservation. If a triangle has an additional connection, as have been pointed out, the coefficients (1) and (2) are taken into accont during the remapping.

After solving the discrete equations and following the remapping we obtain the velocities and energies at the nodes. To obtain the densities and pressures at the nodes (needed only for the remapping at the next cycle), a certain volume must be associated with the node. This volume is defined as

$$V_i = \tfrac{1}{3} \sum_{k(i)} V_k.$$

3.3. *Iterative Procedure*

The momentum equation (6), in which the pressure is given by (10), should be solved by iteration. The iterative procedure is applied separately to velocities and geometrical factors. As to the geometrical factors $\nabla_i V_k^{n+0.5}$ in Eq. (6) and (10), the convergence of iterations does not meet any difficulties. Using Eq. (8), iterations for Eq. (6) rapidly converge if the geometrical factors calculated at the previous iteration are substituted into the right-hand side of Eq. (6). However, if geometrical factors are obtained and frozen, not every iterative process for obtaining velocities $\mathbf{u}_i^{n+1}$ will be convergent. Let $\mathbf{u}_i^{(l)}$ be an approximation to $\mathbf{u}_i^{n+1}$ at the iteration with the number l. If the values $\mathbf{u}_i^{(l+1)}$ are obtained simply by substitution of $\mathbf{u}_i^{(l)}$ into the right-hand side of Eq. (6) this iterative process will converge at a more severe condition than the Courant stability criterion. Therefore, the using of such implicit scheme would not provide any advantage.

We have made use of another iterative procedure. Node i in which calculations are made according to Eq. (6) is separated in the relation (10) in the following way

$$\tilde{P}_k = P_k^n - \left(\frac{\rho_k c_k^2}{V_k}\right)^n \Delta t \left(\mathbf{u}_i^{(l+1)} \nabla_i V_k^{n+0.5} + \sum_{j \neq i} u_j^{(l)} \nabla_j V_k^{n+0.5}\right) + Q_k. \tag{15}$$

After substitution (15) into the right-hand side of (6) and replacing $\mathbf{u}_i^{n+1}$ by $\mathbf{u}_i^{(l+1)}$ in the left-hand side (6) we obtain two equations for the components of vector $\mathbf{u}_i^{(l+1)}$. These equations can be solved without any difficulties. Such an iterative procedure is convergent and the rate of convergence, as can be shown, depends on the quantity

$$b = \operatorname*{Max}_i \left(\frac{1}{m_i} \sum_{k(i)} \frac{\rho_k c_k^2}{V_k} (\nabla_i V_k)^2\right). \tag{16}$$

If a norm of the velocity deviation at iteration l is introduced as

$$\|\delta u^{(l)}\| = \operatorname*{Max}_i |\mathbf{u}_i^{(l)} - \mathbf{u}_i^{(n+1)}|, \tag{17}$$

then it can be obtained that

$$\|\delta u^{(l+1)}\| \leqslant \frac{b \Delta t^2}{1 + b \Delta t^2} \|\delta u^{(l)}\|. \tag{18}$$

So, the iterations are convergent, but the rate of convergence diminishes as Δt grows. The most profitable Δt choice is that in which the Courant condition, taking in our case the form

$$\Delta t < b^{-1/2}, \tag{19}$$

is slightly exceeded. Note that the time-step size Δt according to (16) and (19) is associated with some dimension averaged over several zones rather than with the minimum dimension of triangles. While solving Eq. (6) at a certain time level, several iterations have been required to achieve convergence accuracy of about 1%.

After the velocity field calculation by the iterative procedure, the final pressures $\tilde{P}_k$ are calculated and substituted into the right-hand sides of Eqs. (6) and (9). Only after this the final velocities and energies are found. In this case the energy conservation is exact and is unaffected by the accuracy of iterations.

Along with criterion (19), the time-step Δt is restricted by the condition resulting from the use of an artificial viscosity

$$\Delta t < -\beta \operatorname*{Min}_k \frac{V_k^n}{\sum_{j(k)} \mathbf{u}_j^n \nabla_j V_k^n}. \tag{20}$$

The coefficient β here depends on the coefficient ε in the expression for the artificial viscosity (12). We have taken the values $\varepsilon = 0.5$ and $\beta = 0.5$. This provides sufficient pressure smoothness after the shock front with acceptable shock thickness.

4. NUMERICAL RESULTS

4.1. *Interaction of a Shock with a Low Density Layer*

If a thin gas layer of a low density (heated layer) is located perpendicular to a moving shock front, a precursor will arise in the heated layer and propagate ahead of the main shock. Recently this problem has been causing great interest. For a planar shock generated by a piston the problem has been numerically investigated in [17] with the Eulerian FCT method [18]. The numerical simulation has shown the flow to be self-similar. We have repeated one of the calculations [17] and have obtained good agreement of the results.

Here we consider a similar problem for the shock generated by an impulsive load at the free boundary of an ideal gas occupying a half space. Figure 2 illustrates the initial conditions. The energy is instantaneously released in the region at the free surface which is located along Y-axis. This results in a shock wave moving into the gas and a flow into vacuum. A gas layer of low density ρ_1 (in comparison with the density of the background gas ρ_0) is located perpendicular to the free boundary along X-axis. This layer has the same pressure as the surrounding gas. In the absence of the heated layer the motion after a sufficiently long time becomes self-similar (for an infinite strength shock) [19]. Such a one-dimensional problem has an exact analytic solution if the specific heat ratio $\gamma = \frac{7}{5}$.

If the heated layer is very thin and, hence, there is no new dimensional parameter, the problem must also be self-similar. In this case the flow becomes two-dimensional because the velocity of the shock moving along the heated layer is greater than that of the main shock moving into the background gas. So the existence of the infinitely thin layer leads to the formation of the precursor and the large-scale restructuring of the flow.

The Lagrangian method has an obvious advantage in this problem because of the free boundary. The initial grid was

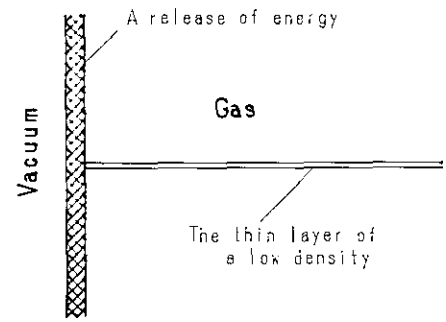

FIG. 2. Intitial conditions in the problem of the shock wave/heated layer interaction.

composed of right triangles and had 40×45 points. We introduced either a uniform, 1.73 times stretched along the X-axis, or a nonuniform mesh in which distances between the nodes grew along X and Y directions in a geometric progression. The points with a low density $\rho_1 = 0.25\rho_0$ were situated in three layers along the X-axis, which was adopted as a rigid wall. The masses of these points were lower than those of the points of the background gas proportional to their densities. The impulsive load initial energy was released in two computational layers near the free surface. Fragments of the Delaunay mesh and the flow velocity field are illustrated in Figs. 3 and 4. The main shock propagates along the X-axis in accordance with the exact solution [19]. The flow behind the precursor is characterized by a vortex motion and interior shocks. The particularities of the flow can be seen in Fig. 4, as well as in Fig. 5, where pressure contours are plotted.

The Lagrangian method allows to see most easily and naturally what gas particles form a precursor. The low density layer points and those of the background gas at a distance from X-axis that is equal to two low density layers are marked in Fig. 6. The space behind the precursor is seen to be filled by the background gas points travelling across the oblique shock front.

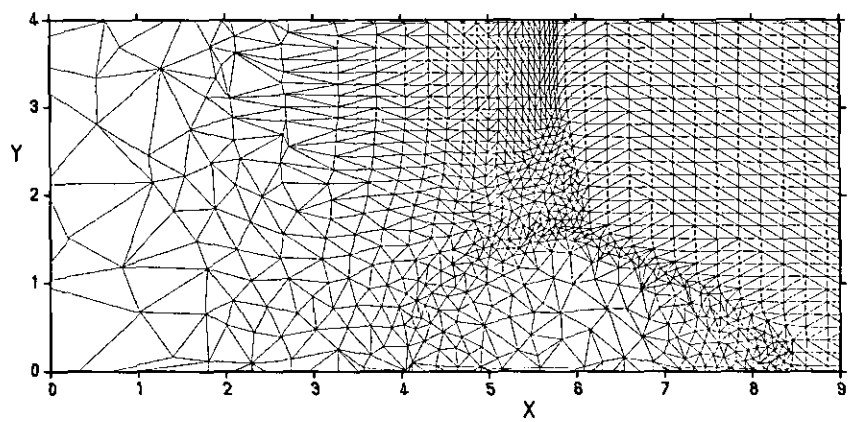

FIG. 3. A portion of the triangular mesh in the problem of the shock wave/heated layer interaction.

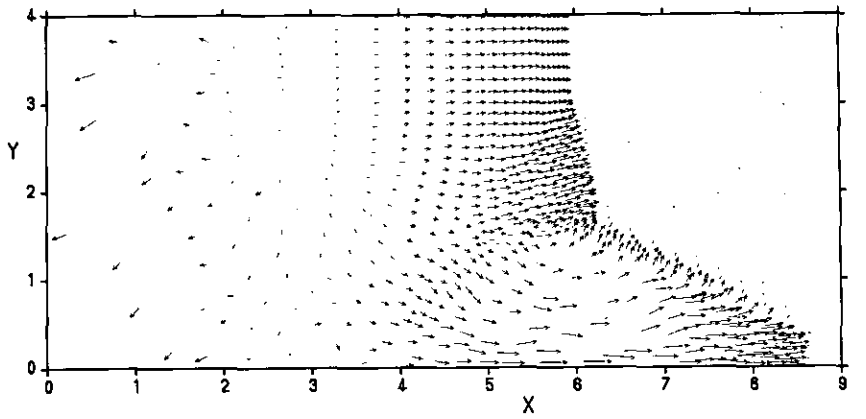

FIG. 4. A flow velocity field in the problem of the shock wave/heated layer interaction.

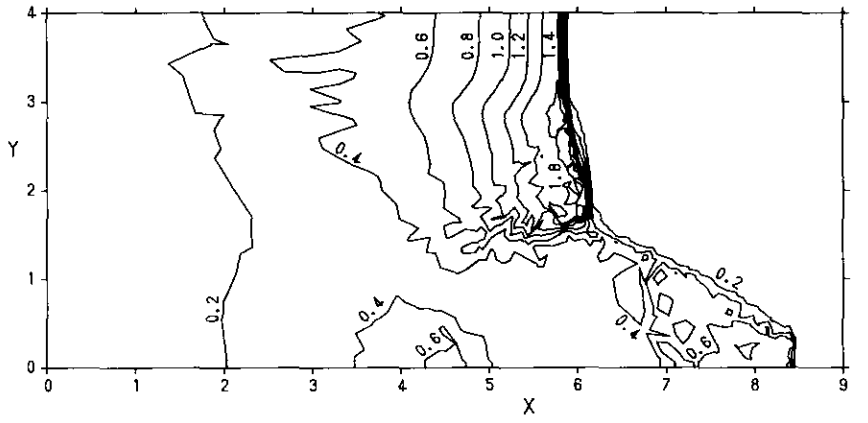

FIG. 5. Pressure contours in the problem of the shock wave/heated layer interaction. The numbers indicate pressure values.

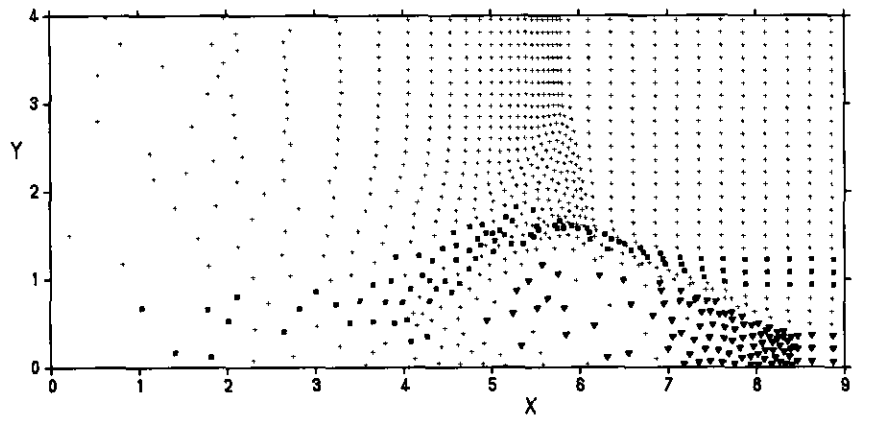

FIG. 6. Marking of particles in the problem of the shock wave/heated layer interaction. The points of the background gas are marked by crosses, the points of the low density layer by triangles, and some distinguished points of the background gas by squares.

The numerical solution on the nonuniform grid with the ratio of subsequent mesh intervals equal to 1.15 has enabled the solution time interval to be enlarged and a tendency to similarity to be obtained with better accuracy. The slope angle ω of the oblique shock obtained in our calculation satisfies an approximate relation [17]

$$\sin^2 \omega = \rho_1/\rho_0.$$

The precursor distance from the initial free surface position $X=0$ is proportional to that travelled by the main shock. The ratio of these distances is 1.35 within a numerical error of about 3%. This constant ratio substantiates the self-similar character of the flow.

4.2. *Meshkov–Richtmyer Instability*

Examples of the Meshkov–Richtmyer instability simulations by free-Lagrangian methods have been presented in [1, 3, 6]. Here we have accomplished calculations corresponding to the recent experiments [20]. In these experiments two different gases—xenon and argon—at a pressure of 0.5 bar have been initially separated in a shock tube by a thin film of sinusoidal shape. The sinusoid wavelength has been varied. An interface instability up to a turbulent intermixing has been caused by an incident shock with the Mach number of about 3.5.

Results of our calculation where the shock travels from the light to heavy gas in the X-axis direction are illustrated in Figs. 7–8. The initial grid consisted of 80×20 nodes. The grid layers near the interface were shifted along the shock tube axis (X-axis) to get a smooth transition to the sinusoidal shape of the layers which form the interface. The sinusoidal interface wavelength was 3.6 cm, and the amplitude was 0.5 cm. Far from the interface the mesh steps were elongated along the X-axis with two factors—1.1 and then 1.2.

Time $t=0$ is settled for a beginning of the shock-interface interaction. Figure 7 demonstrates the compressed triangular mesh behind the shock to the left of the interface and an undisturbed mesh to the right. A velocity field is uniform behind the shock, velocities correspond to the speed of the piston, and the shock front is flat. At $t=137$ mks (Fig. 8) the interface starts to change, having a characteristic "mushroom" form. A penetration of the heavy gas particles into the light gas is seen near the edge of the "mushroom's cap." This picture is in complete accordance with a dark-field shadowgram presented in [20], both the form of the interface and the shock location being in good agreement with the experiment.

The described computational example corresponds to the intermediate wavelength of the interface. At larger wavelengths, both in [20] and in the calculations, the interface remained smooth without changing and at smaller wavelengths an intensive gas intermixing arose near the perturbed interface.

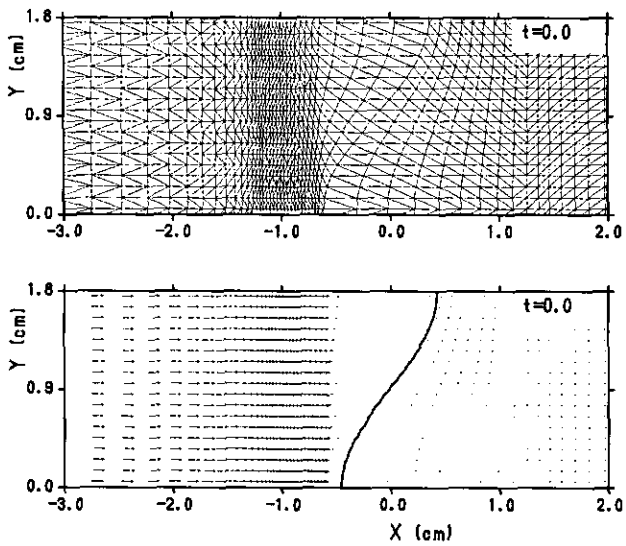

FIG. 7. A triangular mesh and velocity field at $t=0$ when the shock reaches the interface in the problem of Meshkov–Richtmyer instability. The argon/xenon interface is marked out by a thick solid line.

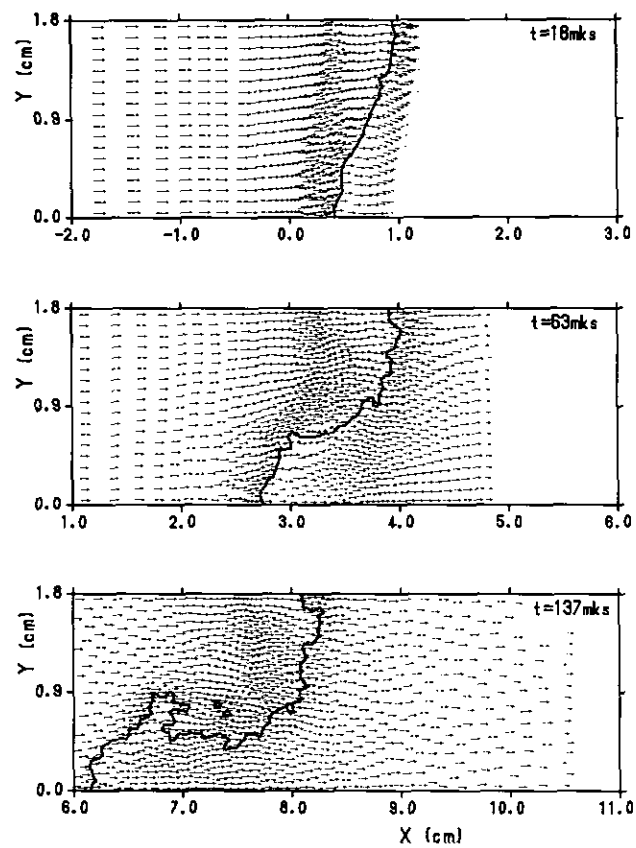

FIG. 8. An interface distortion after the shock as the Meshkov–Richtmyer instability grows.

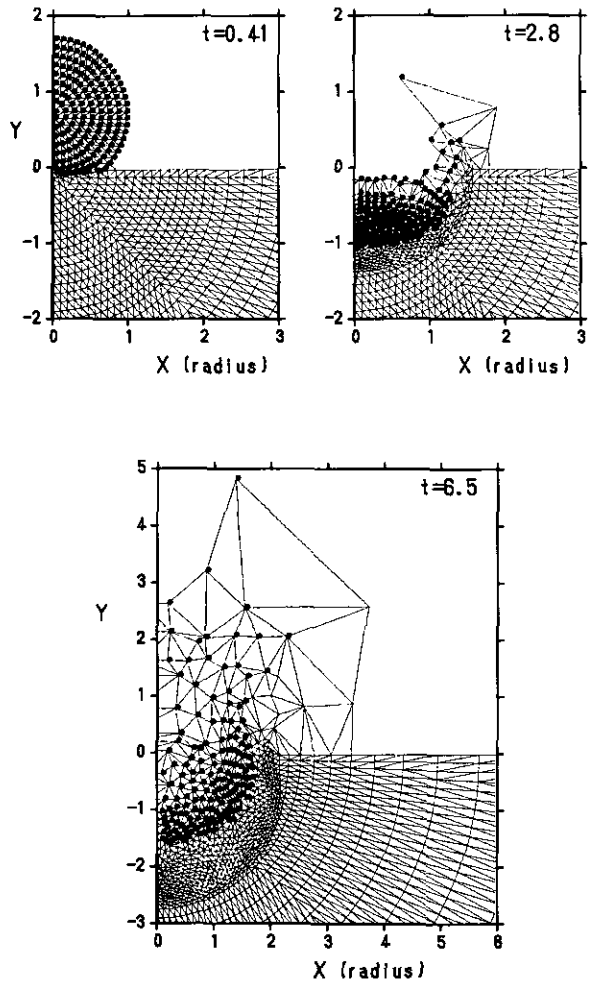

FIG. 9. The projectile impact with a unit velocity on the surface. The impactor points are marked by circles.

4.3. *A Projectile Impact on a Material Surface*

The free-Lagrangian methods are traditionally used for calculations of impacts on various targets [1, 3]. To test our method we have chosen the problem of a cosmic body impact on a planetary surface. This problem has been solved by the Eulerian method in [21] for various densities and velocities of impact using a real equation of state. After repeating some of the calculations [21] we have obtained similar results.

Figure 9 shows our numerical results for the simplified problem in which the impactor and target materials are assumed to be an ideal gas with $\gamma = 2$. In this case the solution does not depend on the impactor velocity. An ideal gas assumption becomes more accurate the higher is the impactor velocity. We took the ratio of a planetary density to the impactor density to be 3, simulating an impact of a comet nucleus. The results proved to be close to the results [21] for 1 g/cm^3 ice projectile impacting a silicate surface at a velocity of 15 km/s.

The grid was constructed with 180 points to define the projectile and 1600 points to define a half space of the target. The points were located on concentric circumferences with centers in the impactor symmetry center and in the impact point. Initially the projectile nodes were detached from the target except for the two nearest points which were connected with the target surface by two triangles. The other projectile points were connected with the surface while the projectile became closer to the target.

The case of constant γ is of interest from the code testing point of view because the solution after a sufficiently long time becomes self-similar [19]. A transition to similarity can be seen in Fig. 9 for the latest time. The shock has a bowl shape that is typical for the self-similar solution of this problem.

4.4. *Expansion of a Thin Cylinder Shaped Foil*

A problem of laser-heated thin exploding foils has been recently considered in [22]. A numerical hydrodynamics simulation has been performed to study an expansion of long thin aluminum ribbons. We consider here an explosion of a short cylinder-shaped foil. A hollow cylinder with a 2-unit height, the same diameter, and a wall 0.01 thick is assumed to be instantaneously vaporized, and its material

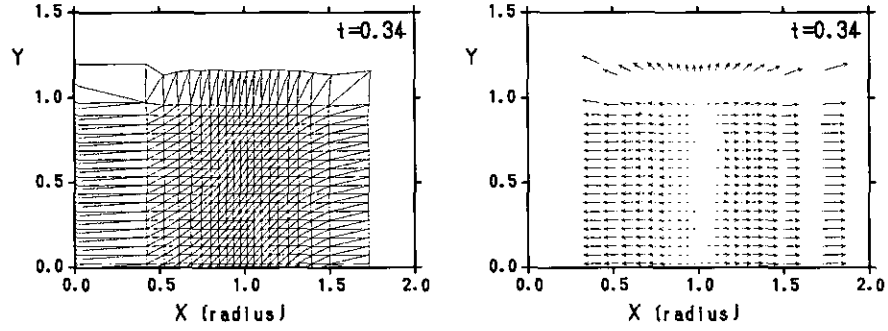

FIG. 10. A triangular mesh and velocity field before reflection of the foil particles from the symmetry axis.

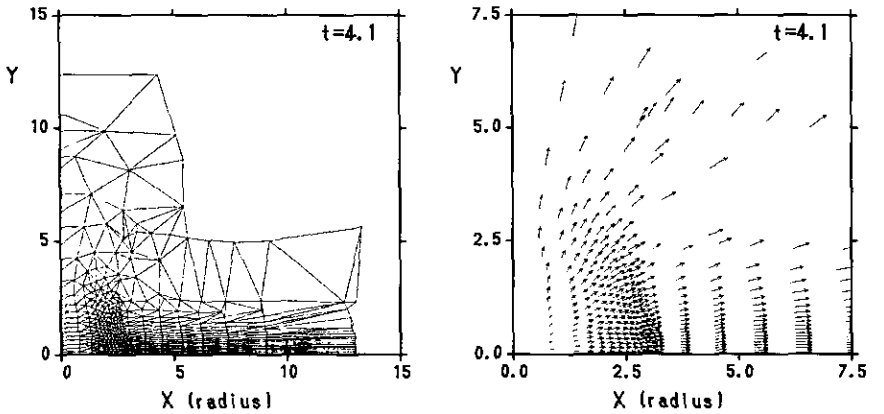

FIG. 11. A formation of jets spreading into vacuum during expansion of cylindrical foil.

becomes an ideal gas with $\gamma = 1.2$. The grid of 20×20 nodes was strongly compressed in the radial direction at the beginning. The cylinder expansion is illustrated in Figs. 10–12.

After the particles reflection from the symmetry axis (Y-axis) a low density jet is formed, spreading initially in the axial direction and then gaining radial velocity. In the radial direction a shock propagates occupying a part of the jet spreading in front of it. Note that a portion of this jet spreading radially preserves almost one-dimensional character, the triangular cells being strongly elongated. Figure 12 shows the expansion inertial stage when the pressure does not appreciably affect the motion. Thus the central part of the radial jet formed at the initial times will continue its motion, unaffected by other particles, up to infinitely large times. The solution of this problem at late times depends on the initial data.

It should be noted that the triangulation in Figs. 11 and 12 is not strictly that of Denaunay in all the regions of the flow. For the stretched cells, as pointed out above, the Delaunay triangulation is applied to the compressed mesh. This takes place in Figs. 11 and 12.

5. CONCLUSIONS

The CSSEL method has proved to be very effective for fluid flow calculations. The mesh flexibility combined with the enhanced intrinsic smoothness and stability have allowed the method to be applied to problems with a relatively complex internal structure of the flows. No additional artificial remedies have been required to improve the numerical solution. In the examples demonstrated the method has provided an adequate description of free expansion, vortex motion, shock interactions, and other important aspects of the flows. However, as in other Lagrangian methods, the computer time proves to be greater than for an Eulerian method if the same number of nodes is used. But the necessary number of points for many problems is much smaller if the free-Lagrangian method is employed.

It took several years to design our modification of the method and obtain a robust code. In the near future we intend to include in the code additional equations for such physical phenomena as heat conduction, emission of radiation, and gravitational attraction.

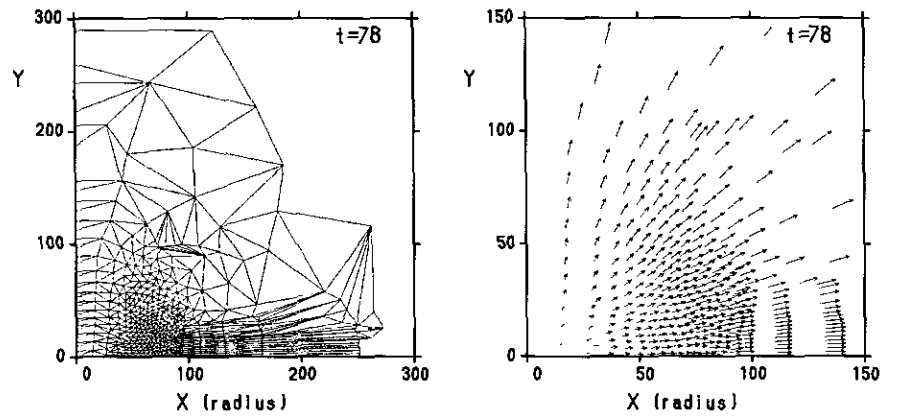

FIG. 12. The late stage of the foil expansion.

ACKNOWLEDGMENT

We thank I. V. Nemchinov who drew our attention to the problems described.

REFERENCES

1. W. P. Crowley, *Comput. Phys. Commun.* **48**, 51 (1988).
2. M. J. Fritts, *Comput. Phys. Commun.* **48**, 75 (1988).
3. R. A. Clark, in *The Free-Lagrange Method*, edited by M. J. Fritts *et al.*, Lecture Notes in Phys., Vol. 238 (Springer-Verlag, New York, 1985), p. 281.
4. I. V. Nemchinov and V. M. Hazins, *Izv. Akad. Nauk SSSR, Mekh. Zhidk. Gaza* **6**, 131 (1982).
5. W. F. Noh, *J. Comput. Phys.* **72**, 78 (1987).
6. W. P. Crowley, in *The Free-Lagrange Method*, edited by M. J. Fritts *et al.*, Lecture Notes in Phys., Vol. 238 (Springer-Verlag, New York, 1985), p. 1.
7. A. H. Armstrong, in *The Free-Lagrange Method*, edited by M. J. Fritts *et al.*, Lecture Notes in Phys., Vol. 238 (Springer-Verlag, New York, 1985), p. 255.
8. J. J. Monagan, *J. Comput. Phys.* **82**, 1 (1989).
9. J. K. Dukowicz, M. C. Cline, and F. L. Addessio, *J. Comput. Phys.* **82**, 29 (1989).
10. V. M. Goloviznin, A. A. Samarskii, and A. P. Favorskii, *Dokl. Akad. Nauk SSSR* **235**, 1285 (1977).
11. B. Delaunay, *Bull. Acad. Sci. USSR (VII), Cl. Sci. Math. Nat.* **793** (1934).
12. G. Voronoi, *J. Reine Angew. Math.* **134**, 198 (1908).
13. M. J. Fritts and J. P. Boris, *J. Comput. Phys.* **31**, 173 (1979).
14. Yu. P. Popov and A. A. Samarskii, *Zh. Vycisl. Mat. Fiz.* **9**, 953 (1969).
15. S. M. Barhrah, G. V. Zharova, and V. F. Spiridonov, *Vopr. At. Nauki Tekh.* **3** (11), 15 (1982).
16. J. Von Neumann and R. D. Richtmyer, *J. Appl. Phys.* **21**, 232 (1950).
17. V. I. Bergelson, I. V. Nemchinov, T. I. Orlova, V. A. Smirnov, and V. M. Hazins, *Dokl. Akad. Nauk SSSR* **296**, 554 (1987).
18. D. L. Book, J. P. Boris, and K. Hain, *J. Comput. Phys.* **18**, 248 (1975).
19. Ya. B. Zel'dovich and Yu. P. Raizer, *Physics of Shock Waves and High-Temperature Hydrodynamics Phenomena, Vol. 2.* (Academic Press, New York, 1966), p. 827.
20. A. N. Aleshin, E. G. Gamalii, S. G. Zaitsev, E. V. Lazareva, I. G. Lebo and V. B. Rozanov, *Pis'ma Zh. Tekh. Fiz.* **14**, 1063 (1988).
21. J. D. O'Keefe and T. J. Ahrens, *J. Geophys. Res.* **87**, 6668 (1982).
22. J. H. Hunter and R. A. London, *Phys. Fluids* **31**, 3102 (1988).